Optogenetic determination of the myocardial requirements for extrasystoles by cell type-specific targeting of ChannelRhodopsin-2

Tania Zaglia[a,b,1], Nicola Pianca[a,b,1], Giulia Borile[a,b], Francesca Da Broi[b], Claudia Richter[c], Marina Campione[a,d], Stephan E. Lehnart[e,f], Stefan Luther[c,e,f,g], Domenico Corrado[h], Lucile Miquerol[i], and Marco Mongillo[a,b,d,2]

[a]Department of Biomedical Sciences, University of Padova, 35122 Padova, Italy; [b]Venetian Institute of Molecular Medicine, 35129 Padova, Italy; [c]Research Group Biomedical Physics, Max Planck Institute for Dynamics and Self-Organization, 37077 Gottingen, Germany; [d]Neuroscience Institute, Consiglio Nazionale delle Ricerche, 35121 Padova, Italy; [e]Heart Research Center Göttingen, Clinic of Cardiology and Pulmonology, University Medical Center, 37077 Gottingen, Germany; [f]German Centre for Cardiovascular Research, partner site Göttingen, 37077 Gottingen, Germany; [g]Institute for Nonlinear Dynamics, Georg-August-Universität Göttingen, 37077 Gottingen, Germany; [h]Department of Cardiologic, Thoracic and Vascular Sciences, University of Padova, 35128 Padova, Italy; and [i]Aix Marseille University, CNRS Institut de Biologie du Développement de Marseille UMR 7288, 13288 Marseille, France

Edited by David E. Clapham, Howard Hughes Medical Institute, Boston Children's Hospital, Boston, MA, and approved June 5, 2015 (received for review May 18, 2015)

Extrasystoles lead to several consequences, ranging from uneventful palpitations to lethal ventricular arrhythmias, in the presence of pathologies, such as myocardial ischemia. The role of working versus conducting cardiomyocytes, as well as the tissue requirements (minimal cell number) for the generation of extrasystoles, and the properties leading ectopies to become arrhythmia triggers (topology), in the normal and diseased heart, have not been determined directly in vivo. Here, we used optogenetics in transgenic mice expressing ChannelRhodopsin-2 selectively in either cardiomyocytes or the conduction system to achieve cell type-specific, noninvasive control of heart activity with high spatial and temporal resolution. By combining measurement of optogenetic tissue activation in vivo and epicardial voltage mapping in Langendorff-perfused hearts, we demonstrated that focal ectopies require, in the normal mouse heart, the simultaneous depolarization of at least 1,300–1,800 working cardiomyocytes or 90–160 Purkinje fibers. The optogenetic assay identified specific areas in the heart that were highly susceptible to forming extrasystolic foci, and such properties were correlated to the local organization of the Purkinje fiber network, which was imaged in three dimensions using optical projection tomography. Interestingly, during the acute phase of myocardial ischemia, focal ectopies arising from this location, and including both Purkinje fibers and the surrounding working cardiomyocytes, have the highest propensity to trigger sustained arrhythmias. In conclusion, we used cell-specific optogenetics to determine with high spatial resolution and cell type specificity the requirements for the generation of extrasystoles and the factors causing ectopies to be arrhythmia triggers during myocardial ischemia.

optogenetics | heart | Purkinje fiber | arrhythmia | cardiac ectopies

Aberrant heartbeats, caused by the ectopic depolarization of a group of cardiomyocytes, are associated with a wide range of consequences, from the commonly experienced feeling of "palpitation" to the triggering of potentially lethal ventricular arrhythmias in diseased hearts. Physiological conduction of normal heartbeats is orchestrated by the interaction of at least two functionally and anatomically distinct populations of cardiomyocytes: the working cardiomyocytes and the conduction system (i.e., Purkinje fibers at the ventricular level) (1). The electrotonic coupling of myocardial cells protects the heart from abnormal excitation and allows the effect of spontaneous activity in sparse cardiomyocytes to be "sunk" by the surrounding myocardium. As a result, a minimal "critical" number of cardiomyocytes needs to simultaneously depolarize to prevail over such a protective mechanism and generate conducted beats (2–5). When this occurs, the source-sink mismatch (abnormal depolarization current/myocardial electrotonic sink) is focally overcome, resulting in a premature ventricular contraction (PVC) that, in the presence of arrhythmogenic substrates, may evolve into chaotic and self-sustained ventricular arrhythmias (6, 7). In fact, ventricular tachycardia (VT) and ventricular fibrillation (VF) frequently occur in coronary artery disease during both the acute ischemic phase and the infarct evolution phase and are responsible for most cases of sudden cardiac death (SCD) occurring yearly in the United States of America (8–10).

The tissue determinants of a focal arrhythmic source (i.e., critical cell number, topology) have so far only been estimated using biophysical modeling, suggesting that almost one million cells are required to generate ventricular ectopies in the rabbit heart (4). Moreover, although pharmacologic approaches and single-cell electrophysiological studies have suggested that abnormal activation of the Purkinje fiber network is a likely arrhythmia trigger in both acquired (e.g., myocardial ischemia) and inherited [long QT syndrome (LQTS) and catecholaminergic polymorphic ventricular tachycardia (CPVT)] arrhythmias (11–16), the role of the cardiac conduction system has not been addressed directly in the intact animal so far, mainly due to methodological constraint (17–20). In fact, the experimental technique most commonly used to

Significance

Arrhythmias are potentially life-threatening electrical heart diseases that are difficult to predict and are mostly treated by empirical interventions. The mechanisms of arrhythmia initiation (triggers) are still poorly understood, mostly due to the technical limitations of conventional experimental methods in cardiac electrophysiology. Here, we use optogenetics, a technique based on the expression of photoactivated proteins such as ChannelRhodopsin-2 (ChR2), which allows for noninvasive control of the cell membrane potential through illumination with blue light. By developing mice with cell-specific expression of ChR2, we investigated the role of the different cardiomyocyte types present in the heart and determined the factors triggering arrhythmic beats in the normal heart and during myocardial ischemia, a condition frequently associated with lethal arrhythmias causing sudden cardiac death.

Author contributions: M.M., S.E.L., and S.L. designed research; M.M., T.Z., N.P., G.B., F.D.B., C.R., S.E.L., S.L., and L.M. performed research; M.C. contributed new reagents/analytic tools; M.M., T.Z., N.P., G.B., C.R., S.E.L., S.L., and L.M. analyzed data; and M.M., T.Z., N.P., S.E.L., D.C., and L.M. wrote the paper.

The authors declare no conflict of interest.

This article is a PNAS Direct Submission.

[1]T.Z. and N.P. contributed equally to this work.

[2]To whom correspondence should be addressed. Email: marco.mongillo@unipd.it.

This article contains supporting information online at www.pnas.org/lookup/suppl/doi:10.1073/pnas.1509380112/-/DCSupplemental.

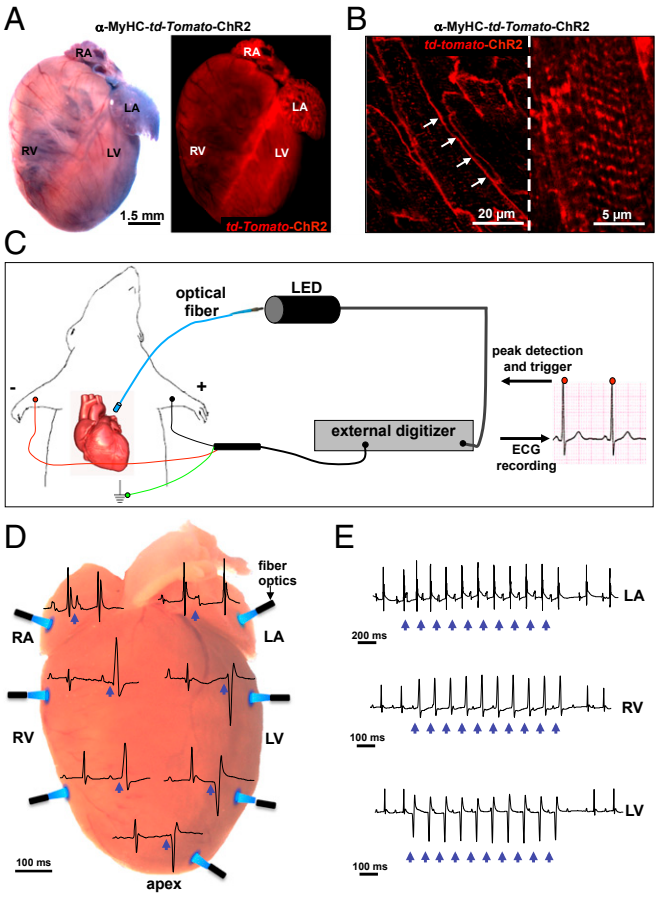

Fig. 1. Cardiac optogenetics allows noninvasive investigation of heart electrophysiology in vivo. (*A*) Bright field (*Left*) and fluorescence (*Right*) images of α-MyHC-*tdTomato*-ChR2 heart. The *Right* image of *tdTomato* fluorescence shows expression of ChR2 in both the atria and the ventricles. LA, left atrium; LV, left ventricle; RA, right atrium; RV, right ventricle. (Scale bar, 1.5 mm.) (*B*) Confocal image of ventricular cryosections from α-MyHC-*tdTomato*-ChR2 transgenic hearts showing ChR2 localization at the level of cardiomyocyte sarcolemma (white arrows) and t-tubuli. (Scale bar, 20 μm; high magnification, 5 μm.) (*C*) Representation of the setup used for epicardial photostimulation in open-chest anesthetized mice. LED stimulation occurred through fiber optics delivering time-controlled pulses of 470 nm blue light. The LED was connected to the ECG apparatus, allowing synchronization of the LED stimulation with a specific time point of the ECG recording. (*D* and *E*) Representative ECG traces of ectopic beats originated by epicardial light stimulation of different regions of the myocardium from α-MyHC-ChR2 mice ($n = 10$ mice). Blue arrows in *D* and *E* indicate light pulses. LA, RV, and LV photostimulation originates ectopic beats with different QRS shape.

investigate cardiac electrophysiology in vivo is based on the delivery of electrical pulses to the epicardial surface during ECG recording (21, 22). The method, however, cannot discriminate the specific role of the conduction system cells, as they are embedded in the myocardium and not easily accessible to invasive electrophysiological investigation (20, 23–25).

Optogenetics exploits the targeting of photoactivatable ion channels in specific cell types to achieve noninvasive control of membrane potential (26).

Channelrhodopsin-2 (ChR2) is a microbial-derived cation channel that, in a similar way to visual rhodopsin and bacteriorhodopsin, undergoes a conformational change upon illumination, resulting in an immediate increase in ionic permeability, with high conductance to Na^+ (27, 28). ChR2 exhibits fast and reversible activation kinetics (in the order of milliseconds) that is instrumental to drive reliable trains of high-frequency action potentials in vivo. Optogenetics is widely used in neuroscience to modulate neuronal circuits in in vivo models (29–31) and has been proposed as an attractive tool to control cardiomyocyte membrane potential (32–36). In cardiac research, optogenetics is still in the very early stages and has mainly been applied to in vitro and regenerative medicine studies (37–41).

We have applied optogenetics in transgenic mice with cardiac-specific ChR2 expression to determine the critical cell mass necessary to generate focal ectopic beats ex vivo, in the isolated heart, and in vivo. In addition, we addressed the vulnerability of the ischemic heart to ventricular arrhythmias, in relation to the characteristics of the focal trigger. Furthermore, we exploited genetic targeting of ChR2 to Purkinje cells to interrogate the role of this cellular network in cardiac electrophysiology and arrhythmogenesis.

Results

Noninvasive Generation of Cardiac Ectopies in Vivo Using Cardiomyocyte-Specific Expression of ChR2. To achieve ChR2 expression in cardiomyocytes, we crossed B6.Cg-Gt (ROSA) 26Sortm27.1$^{(CAG\text{-}COP4*H134R/tdTomato)\ Hze}$/J-expressing mice with a transgenic strain encoding Cre-recombinase under the control of a cardiac-specific α-Myosin Heavy Chain (α-MyHC) promoter. The resulting offspring had the STOP cassette deleted in cardiomyocytes, driving the expression of ChR2 [hChR2 (H134R)-*tdTomato* fusion protein] (Fig. S1*A*). ChR2 expression was uniformly detected in heart cryosections by *tdTomato* fluorescence and was localized at the sarcolemma and t-tubules of cardiomyocytes (Fig. 1 *A* and *B* and Fig. S1*B*). ChR2-expressing mice had normal heart size, morphology, and gross electrophysiology [heart rate, α-MyHC-ChR2, 340 ± 39 vs. control, 322 ± 9, in beats per minute (bpm); $n = 10$ mice for each group, under anesthesia] (QRS interval, α-MyHC-ChR2, 12.43 ± 0.63 vs. control, 13.05 ± 0.87, in ms; $n = 10$ mice for each group) (Fig. S1 *C* and *D*).

To obtain timely and spatially controlled photostimulation of ChR2 hearts in vivo, we used a fiber optic delivering 470-nm light pulses, generated by a time-controlled light emitting diode (LED), in open-chest anesthetized mice during continuous ECG monitoring (Fig. 1*C*). The effect of local cardiac photostimulation was mapped by delivering brief (5 ms) light pulses with the fiber tip placed close to the epicardium of different heart regions (Fig. 1 *D* and *E*). Atrial stimulation evoked supraventricular paced beats with normal QRS and wider P waves [P wave duration, basal, 14.28 ± 0.26 vs. left atrium (LA) photostimulation, 27.90 ± 0.63, in ms; $n = 15$ mice]. Ventricular stimulation from the heart base to the apex, in both the right and left sections, triggered beats with wider QRS complexes [QRS interval, basal, 12.43 ± 0.63 vs. left ventricle (LV) photostimulation, 21.82 ± 0.90, in ms; $n = 10$ mice for each group] (Fig. 1*D*). Repetitive stimulation of the same myocardial focus produced paced heartbeats that, consistent with the fixed ventricular origin, had enlarged and identical QRS morphology (Fig. 1*E*). Photopacing could be maintained for several minutes, and sinus rhythm started promptly when illumination was interrupted, suggesting that no functional or structural damage resulted from the activation protocol. In addition, disconnection of the fiber optics tip from the light source on the epicardial surface as well as photostimulation of WT littermates did not cause any alteration in the sinus rhythm.

We thus demonstrated that experimentally induced ectopies can be evoked, using optogenetics, with high spatial and temporal resolution and implemented such methodology for the noninvasive investigation of cardiac electrophysiology.

Voltage Mapping of Cardiac Activation in Optogenetically Paced ChR2 Hearts. To address the effect of light pulses on ChR2 hearts directly at the local tissue level, cardiac optogenetics was combined with high-speed optical mapping of membrane voltage in

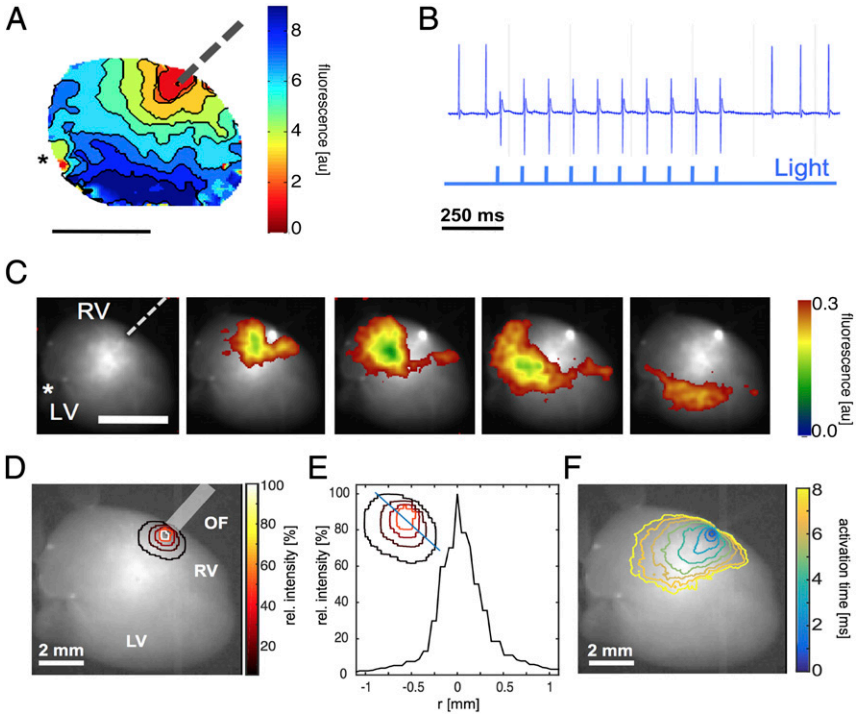

Fig. 2. Optogenetics-based investigation of heart electrophysiology ex vivo. (*A*) Activation map of one photostimulation pulse on the RV. The dashed line indicates the stimulation fiber position. (Scale bar, 0.5 cm; color bar in ms.) (*B*) Example of monophasic potential (MAP) signal during photostimulation. (*C*) Optical mapping (Vm) of one light pulse. The fiber position is represented in the first snapshot by the gray dashed line. All propagations showing snapshots are separated in time by 2 ms. (Scale bar, 0.5 cm.) The asterisk shows the MAP electrode position. (*D–F*) Optical measurement of photostimulation and spread of activation in a Langendorff-perfused intact mouse heart. (*D*) Intensity distribution of photostimulation using an optical fiber (OF; diameter, 0.4 mm). The position of the fiber tip is indicated by the gray-shaded rectangle. The isochrones indicate the relative intensity (colors of the isochrones correspond to the color bar). LV, left ventricle; RV, right ventricle. (*E*) Cross-section of the intensity distribution. The intensity profile is given along the blue line shown in the *Inset*. (*F*) Activation map showing the propagation of wave fronts following photostimulation.

Langendorff-perfused mouse heart preparations. To achieve this, isolated hearts from α-MyHC-ChR2-tg mice were loaded with a voltage-sensitive membrane dye (RH1691) and monophasic action potentials were recorded in parallel by a contact electrode from the heart surface (Fig. 2 *A* and *B* and Fig. S2). Light pulses achieved with the same optics used for in vivo experiments caused reproducible local depolarizations that, strictly within the time window of the light pulse, were confined to a tissue area corresponding precisely to the optical fiber physical diameter. Moreover, the radial intensity distribution of photostimulation light applied was initially symmetric and well-confined to the radius of the optical fiber, with no appreciable fluorescence changes at the margin of the photostimulated area. Furthermore, considering the dynamic range of the voltage dye and the given signal-to-noise ratio of the optical system, voltage changes at the edge of the region directly irradiated were below 1 mV. Above a light intensity threshold comparable to that observed in vivo, optical pacing resulted in an activation pattern that was initially of radial symmetry and subsequently developed a physiological, anisotropic propagation spread as shown in Fig. 2 *C–F*. Taken together, the combined measurement of optogenetic tissue activation and epicardial voltage mapping shows that local light delivery to ChR2-expressing hearts activates a relatively small tissue volume that precisely correlated with the light source and triggers focal ectopic beats or tertiary pacemakers. These proof-of-principle ex vivo data support the all-optical approach to simultaneously control light switches focally in cardiac tissue and to record the corresponding local electrophysiological activity.

Direct Optogenetic Assessment of Purkinje Fiber Function in Vivo Using Cx40-Driven Expression of ChR2. The Purkinje fiber network constitutes the distal ventricular conduction system, branching throughout the subendocardial cell layers of both ventricles, with a high density in the right ventricular (RV) wall. In vitro studies and mathematical modeling indicate that Purkinje fiber cells have unique structural and electrophysiological properties, but the direct assessment of their function in vivo, with conventional approaches (i.e., electrical stimulation), is limited by their subendocardial location and proximity to surrounding working cardiomyocytes. To interrogate the specific role of Purkinje fiber myocytes in heart physiology, we genetically targeted ChR2 expression to the ventricular conduction system cells. Double-floxed *ChR2-tdTomato* mice were crossed with Connexin-40 (Cx40)-Cre mice, previously shown to drive transgene expression throughout the conduction system cells, including Purkinje fibers, and atrial myocardium (42) (Fig. 3*A*). ChR2 expression was assessed by confocal imaging of the red fluorescence of *td-Tomato*, and its specific expression by Cx40-expressing cells was confirmed by immunofluorescence. ChR2 was thus detected in atrial cardiomyocytes and Purkinje fibers, consistent with the expression of Cx40 (Fig. 3 *B–D* and Fig. S3). Hearts from Cx40-ChR2 mice had normal morphology and function (heart rate, Cx40-ChR2, 351 ± 20 vs. control, 335 ± 15, in bpm; $n = 10$ mice for each group) (QRS interval, Cx40-ChR2, 12.82 ± 0.25 vs. control, 12.35 ± 0.47, in ms; $n = 10$ mice for each group), indistinguishable from control littermates (Fig. S4 *A* and *B*).

We therefore used the photoactivation protocol described above (Fig. 1*C*) to selectively stimulate, by illuminating the epicardial surface, discrete foci of Purkinje fibers in the intact heart in vivo and analyze the effects on cardiac electrical activation. Consistent with the ubiquitous expression of ChR2 in atrial cells, photoactivation of the right atria (RAs) and LAs resulted in supraventricular pacing, with ECG morphology superimposable to that

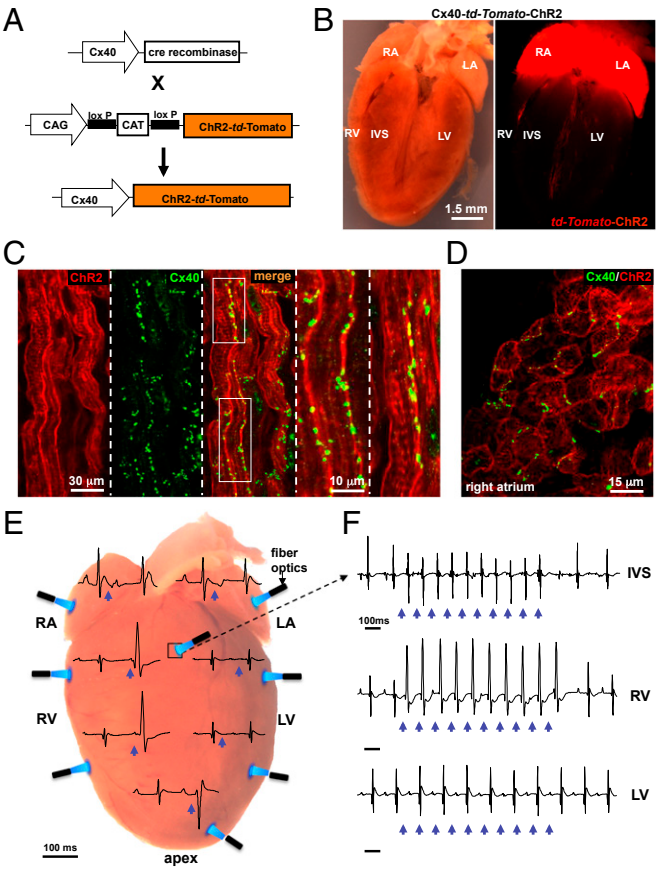

Fig. 3. Direct optogenetic assessment of Purkinje fiber function in vivo. (*A*) Scheme of the generation of the transgenic mouse expressing the fused protein *tdTomato*-ChR2 under the control of the Cx40 promoter (Cx40-ChR2). (*B*) Bright field (*Left*) and fluorescence (*Right*) images of a longitudinally sectioned whole Cx40-ChR2 heart. The *Right* image shows specific expression of ChR2 in the atria and the conduction system. LA, left atrium; LV, left ventricle; RA, right atrium; RV, right ventricle. (Scale bar, 1.5 mm.) (*C* and *D*) Confocal immunofluorescence analysis on ventricular (*C*) and atrial (*D*) cryosections from red fluorescent Cx40-ChR2 mice stained with an antibody specific for Cx40 (green signal). [Scale bars, (*C*) 30 µm, and high magnifications, 10 µm; (*D*) 15 µm.] (*E* and *F*) Representative ECG traces of ectopic beats originated by epicardial photostimulation of different regions of the myocardium from Cx40-ChR2 mice ($n = 8$ mice). Blue arrows indicate light pulses. RV and interventricular septum photostimulation originates ectopic beats with different QRS shapes in all mice, whereas LV epicardial stimulation always failed to induce ectopies.

obtained in the α-MyHC-ChR2 transgenic hearts at corresponding pacing sites (Fig. 3*E* and Fig. S4*C*). By scanning the heart surface with the fiber optic tip, the ventricular conduction system was activated at different sites, corresponding to proximal (septal) and distal regions of the Purkinje fiber network, both in the RV and LV. Consistent with the physiological characteristics of the different conduction system regions, ectopies triggered by photoactivation of the atrio-ventricular bundle had QRS duration identical to the spontaneous complex (Cx40-ChR2 basal QRS, 12.82 ± 0.25 vs. photostimulated QRS, 13.04 ± 0.33, in ms; $n = 10$ mice for each group) (Fig. 3*F*). Although stimulation of the distal Purkinje fibers of the RV yielded ectopic beats with enlarged QRS duration (photostimulated QRS duration, 23.2 ± 0.52, in ms; $n = 10$ mice for each group), light pulses failed to activate ectopies when delivered to the much thicker LV wall (Fig. 3 *E* and *F*).

In contrast to the uniform response to photoactivation of the α-MyHC-ChR2 ventricles, Purkinje fiber stimulation yielded highly variable effects depending on the illumination site. Ectopies were in general evoked with the stimulation of all RV regions, however successfully coupled light pulses were almost 100% in a small (about 2 mm^2 wide) region of the lateral RV free wall (Figs. 3 *E* and *F* and 4*A*), corresponding to the origin of the RV outflow tract (RVOT). We thus used confocal immunofluorescence and optical projection tomography in intact Cx40-GFP mouse hearts to investigate the relationship between the geometry of Purkinje fiber arborization and the response to photostimulation. The small RV hyperactivable region identified functionally with optogenetics (Fig. 4*A*) was characterized by the presence of Purkinje fibers arranged in multiple cell layers (Fig. 4*B*). Moreover, the 3D reconstruction of the ventricular conduction system network showed that, in this region, Purkinje fibers of the RV free wall connect to the right septal branch (Fig. 4 *C*–*F*), suggesting that the

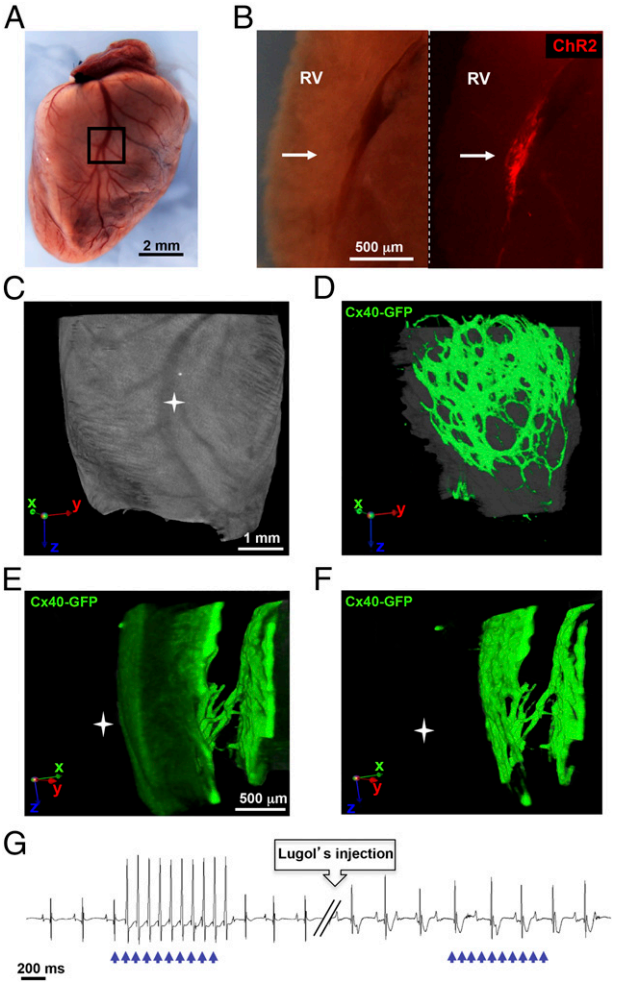

Fig. 4. Correlation between distribution and function of the Purkinje fiber network in the RV. (*A*) RV epicardial surface from a whole Cx40-ChR2 heart. The black box indicates the RV region with the highest responsiveness to photostimulation. (Scale bar, 2 mm.) (*B*) Bright field (*Left*) and fluorescence (*Right*) images of the RV section at the anatomical level enclosed in the black box in *A*. (Scale bar, 500 µm.) (*C*–*F*) 3D reconstruction of the RV Purkinje fiber arborization obtained in Cx40-GFP transgenic mice by optical projection tomography. Rotation of the 3D reconstructed image (see coordinates in the panel corner) (*E* and *F*) highlights the connecting bundle between the septal and the RV branches of PF. (*G*) Representative ECG traces of ectopic beats originated by epicardial light stimulation of the RV from Cx40-ChR2 mice before and after (15 min) RV intracavital Lugol's solution injection ($n = 5$ mice). Blue arrows indicate the light pulses. Lugol's solution treatment caused enlargement of the QRS complex and abolished light-induced ectopies in all mice analyzed.

increased responsiveness to local activation might be explained by the high degree of interconnection between sectors of the conduction system. Regardless of the photoactivation site or intensity, the response to RV photoactivation of Cx40-ChR2 hearts was abolished by intracavital injection of iodine/potassium iodide solution (Lugol's solution), a common strategy used to ablate Purkinje fibers (11, 43–47), further proving the specificity of the Cx40-ChR2 mouse model (Fig. 4*G*).

Our results show that the Cx40-ChR2 model represents a unique tool to investigate the role of the cardiac conduction system in vivo, using a simple experimental setup that allows accuracy and flexibility without requiring invasive approaches (i.e., endocardiac electrophysiology).

Selective Electrophysiological Study of Purkinje Fibers in Vivo. To assess the maximal ventricular pacing rate, we photostimulated hearts with trains of light pulses delivered at an incrementally shorter cycle repetition rate, from 10 to 25 Hz, and determined the threshold for 1:1 capture by analyzing the ECG trace. The α-MyHC-ChR2 hearts were responsive up to 18 Hz (1,080 bpm) (n = 5 mice), whereas the Cx40-ChR2 mice responded with 1:1 capture up to about 15 Hz (900 bpm) (n = 5 mice), and above this threshold, stimulation was effective in a variable percentage of activation flashes (Fig. 5*A*). These results are compatible with the increased refractoriness reported for conduction system cells with respect to working cardiomyocytes. However, the effective refractory period (ERP) of Purkinje fibers has only been determined in ex vivo preparations (15, 45, 48–51) or inferred using intracavital microelectrodes to deliver electrical pulses to an area that includes, but is not limited to, the conduction system (23–25, 52, 53). We thus performed noninvasive epicardial optical programmed stimulation to determine selectively the ERP of Purkinje fibers and that of the working cardiomyocytes in vivo. The standard electrophysiological protocol of "extrastimulus" (*Methods* and Fig. 5*B*) was used for optical stimulation. In agreement with the data acquired using ex vivo preparations, the ERP of Purkinje fibers, measured directly in vivo, was significantly longer than that of the working myocardium (ERP, RV Cx40-ChR2, 59.7 ± 1.2 vs. α-MyHC-ChR2, 38.4 ± 2.6, in ms; n = 5 Cx40-ChR2 mice and n = 10 α-MyHC-ChR2 mice) (Fig. 5*C*). This latter value was indistinguishable from those values obtained with conventional electrical stimulation (54).

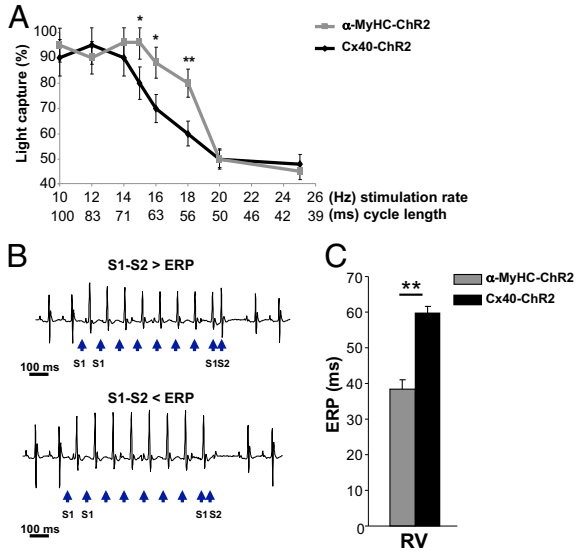

Fig. 5. Optogenetics allows selective interrogation of Purkinje fiber electrophysiology in vivo. (*A*) Stimulation rate/cardiac capture relationship obtained in α-MyHC-ChR2 and Cx40-ChR2 mice. Bars represent SEM (*P < 0.05, **P < 0.01; n = 5 mice for each group). (*B*) Optical programmed stimulation using the extrastimulus (S1 and S2) protocol to measure the ERP. Blue arrows indicate the light pulses. (*C*) Evaluation of the ERP in the RV of both α-MyHC-ChR2 (gray bar) and Cx40-ChR2 (black bar) mice. Bars represent SEM (**P < 0.01; n = 10 α-MyHC-ChR2 mice and n = 5 Cx40-ChR2 mice).

Requirement for Afterdepolarizations to Trigger Ectopies in the Working Versus Conducting Myocardium. Propagation of focal arrhythmic beats in the heart occurs when the current density generated by the abnormally depolarizing cardiomyocytes (current source) is sufficient to overcome the electrotonic sink of the surrounding polarized tissue. The critical cell number needed to bring the sink to its activation threshold has never been determined directly in the intact heart. Similarly, the individual contribution of the two distinct myocyte populations (i.e., working vs. Purkinje myocytes) has not been elucidated. Here, we exploited the ability of optogenetics to specifically control a distinct myocardial cell population, in a well-defined volume, to determine the tissue requirements for the generation of a globally spreading wavefront causing arrhythmic beats in vivo.

Calculation of blue light attenuation by the myocardium. The optogenetics experiments were based on the local photoactivation of ChR2 in confined myocardial volumes. Therefore, to calculate the tissue depth irradiated by light at sufficient intensity to activate ChR2, we first sought to determine the blue light attenuation coefficient of the myocardium. To this aim, the fiber optic illuminator was placed on one side of a myocardial slice and the light intensity emerging across the slice was measured with a radiometer (Thorlabs GmbH). The fractional light absorption was estimated for slices of incrementally higher thickness, from 25 to 800 μm. This allowed determination of the light attenuation coefficient of the myocardium by fitting the experimental data to the commonly used light-matter interaction model, Lambert law: $I(h) = I_o e^{-h/\delta}$ (37, 55, 56), where I_0 is the light intensity at the source, h is the depth in the tissue, and δ is the scattering length (Fig. 6*A*). Data fitting gave us a scattering length δ of 240 μm with a good coefficient of determination (R^2 > 0.9). The experimental data obtained for light attenuation were fitted to another light-matter interaction model, the Kubelka–Munk model (57, 58), resulting in the estimate of the scattering parameter S = 14–20 mm^{-1} (the S parameter previously calculated for the brain is 12 mm^{-1}) (57). Based on ChR2 activation threshold values, obtained by us and confirmed by others in isolated cells (1–0.5 mW/mm^2) (35, 37), we were thus able to determine the depth of photoactivated ChR2 into the myocardium in each experimental condition. The physical features of the optic fibers define an emerging light cone with a very narrow opening angle, around 15°, which was calculated from the numerical aperture of the fiber (0.39 for all fibers, with the exception of the 100 μm diameter fiber, which was 0.22) and the refractive index of the myocardium (1.44) (59). Subsequently, to experimentally assess the degree of lateral delimitation of the incident light beam and the effect of tissue light scattering, we captured the image of the light, as emerging from the myocardial slices. The analysis of the beam intensity profile indicates that although the beam shape has the tendency to diverge with distance from the light source, over 90% of total light intensity was confined in a volume that can be approximated to a cylinder (Fig. 6*B* and Fig. S5).

Optogenetic assay of the minimal myocardial volume to obtain PVCs. To quantify the relationship between the number of activated cells and the ability to generate ectopies, we then implemented an optogenetic assay based on gradually increasing the photoactivation light intensity (at the fiber tip) in differently sized fiber optics (light intensity, 0.36–27 mW/mm^2; fiber tip diameter, 100–1,500 μm).

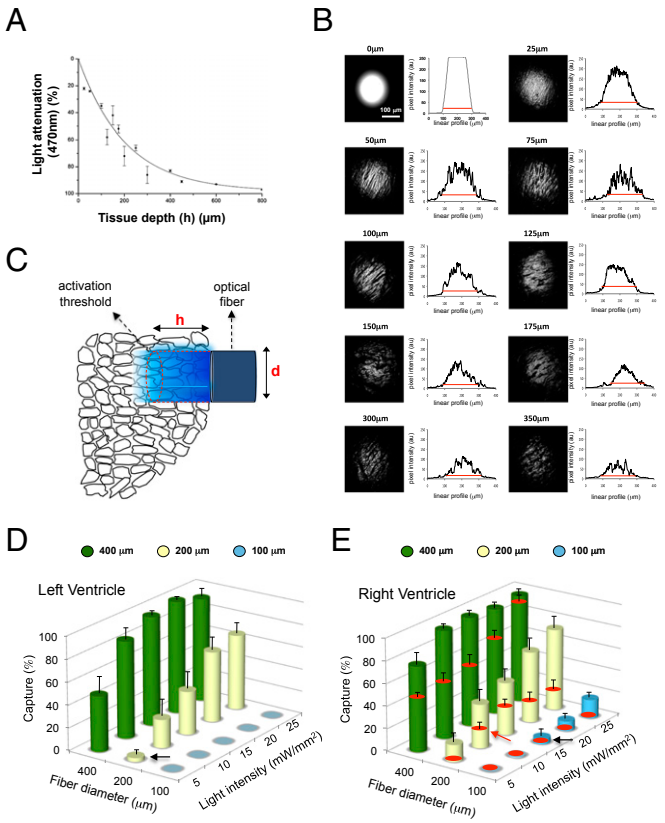

Fig. 6. Optogenetic assay of the minimal myocardial volume required to trigger focal ectopic beats in the normal myocardium. (*A*) Measure of 470 nm light penetrance into the ventricular myocardium upon epicardial illumination. Experimental data were fitted to a monoexponential decay function ($R^2 > 0.9$) (57), shown with a solid line. Bars represent SEM ($n = 10$). (*B*) Images of the optical fiber's light beam, as emerging from myocardial slices of incremental thickness. For each image the beam intensity profile is shown; the red bar indicates the diameter of the optical fiber. (*C*) Modulation of light intensity and fiber diameter shapes the depth (h) and width (d), respectively, of the illuminated myocardial cylinder. (*D* and *E*) Optogenetic assay of minimal myocardial volume required for successful trigger of ectopies in the LV (*D*) and RV (*E*). The red circle in the columns in *E* indicates the percentage of successfully captured beats after Purkinje fiber ablation with Lugol's solution. Black arrows in *D* and *E* indicate the liminal tissue volume to be irradiated to evoke ectopic beats. Red arrow in *E* indicates the liminal tissue volume after Lugol's solution injection in the RV. Bars represent SEM (measures repeated in triplicate, in $n = 10$ mice).

We were thus able to control the light penetration depth (h) and width (d), respectively, thus shaping the volume of illuminated myocardium as shown in Fig. 6*C*. When all cardiomyocytes were photoactivated (α-MyHC-ChR2, $n = 10$ mice), ventricular beats were triggered upon illumination of a minimal tissue volume of 12.6–18 nL (d, 200; h, 400–570, in μm) in the LV and 5.1–5.7 nL (d, 100; h, 650–720, in μm) in the RV, which would result, when considering the average cardiomyocyte volume (10 pL) and orientation in the different cell layers, in about 1,300–1,800 (LV) and 511–570 (RV) cells, respectively (Fig. 6 *D* and *E*). It is likely that the differences observed in the critical tissue mass in the two ventricles may reflect the contribution of Purkinje fibers, mainly found in the subendocardial layers, to the photoactivation of the thinner RV; although, a role played by the different electrophysiological properties of RV and LV cardiomyocytes cannot be excluded. To more specifically establish the critical tissue requirements to generate PVCs upon RV stimulation, we chemically ablated Purkinje fibers using intracardiac injection of Lugol's solution in α-MyHC-ChR2 mice. In these conditions, the minimal photoactivated cell number, in the RV, increased to values comparable to those measured in the LV (RV + Lugol's solution, 1,800–2,300 working myocytes; d, 200; h, 570–740, in μm; $n = 5$ mice) (Fig. 6*E*). Due to the higher thickness of the LV wall, Purkinje fibers failed to be photoactivated with epicardial photostimulation. Consistently, LV intracavital Lugol's solution injection did not cause significant changes in susceptibility to photoactivation and consequently in the minimal tissue volume required for generating an ectopic beat.

It is well established that Purkinje fibers are prone to develop early or delayed afterdepolarizations that, in turn, represent common trigger mechanisms of ventricular arrhythmias. How many Purkinje fiber cells are needed to simultaneously fire, for successful propagation of their AP into the myocardium, has not been determined so far. Thus, we calculated the minimal volume to be irradiated to evoke Purkinje fiber-driven PVCs in the most responsive regions of the RV, which resulted in about a d of 200 and an h of 570–740, in μm, corresponding, based on our immunohistochemical quantification, to about 90–160 cells ($n = 8$ Cx40-ChR2 mice).

Collectively, our results demonstrate that ectopies can be triggered in vivo by the afterdepolarization of either a substantial number of working cardiomyocytes or a much lower quantity of Purkinje fibers. Although with disparities in the cell number presumably due to species differences, our findings support the concept suggested by computational modeling of the rabbit heart, whereby afterdepolarizations arising in Purkinje fibers are more likely to overcome the source-sink mismatch and trigger ectopic beats (4).

Optogenetic Discrimination of Arrhythmia Trigger Sites During Myocardial Ischemia. SCD caused by ventricular arrhythmias in the early phase of acute myocardial ischemia accounts for a large number of fatalities (8). Ischemia induces heterogeneities in excitability, refractoriness, and/or conduction that generate a permissive myocardial environment (substrate) upon which abnormal depolarizations, although uneventful in the healthy heart, may act as a trigger for self-sustained arrhythmias. What the factors are—that is, location relative to the ischemic area, size, and cell type (i.e., working vs. Purkinje myocytes)—that characterize an efficient focal trigger for sustained ventricular arrhythmias during ischemia have not been addressed directly.

To explore this, optogenetics was used during the acute phase of experimental ischemia in α-MyHC-ChR2 and Cx40-ChR2 mice. Myocardial ischemia was obtained by ligating the left anterior descending (LAD) coronary artery, during continuous ECG monitoring. The associated myocardium became immediately pale, and within the first 15 min, ischemia caused the expected alterations in the QRS complex (Fig. S6).

The susceptibility to focal arrhythmia triggering was assessed using a photostimulation protocol consisting of a burst of 10 light pulses (5 ms), at repetition rates from 10 to 20 Hz (cycle length from 100 ms to 50 ms), that was applied to a series of reference epicardial sites of the LVs and RVs (1, LV anterior; 2, LV septal; 3, lateral; 4, RV free wall; 5, septal; at basal, mid, and apical regions). In both the α-MyHC-ChR2 ($n = 10$ mice) and the Cx40-ChR2 ($n = 8$ mice) hearts, responses to focal photostimulation were, in the initial phase (0–15 min), similar to nonischemic controls, with the exception of the anterior LV region, which became progressively unresponsive due to the direct effect of ischemia. Local burst activation at none of the cardiac foci resulted in sustained arrhythmias (Fig. 7 *A* and *B*) (0 out of 10 mice for α-MyHC-ChR2 and 0 out of 8 mice for Cx40-ChR2). At 15–30 min after ischemia, in α-MyHC-ChR2 mice, the identical photostimulation protocol, applied to a restricted area of the RV basal free wall (corresponding to the junctional region between the septal and RV conduction system) (Fig. 4), evoked frequent episodes of nonsustained runs of polymorphic VT, lasting a few beats after pacing in all animals analyzed (Fig. 7 *C*,

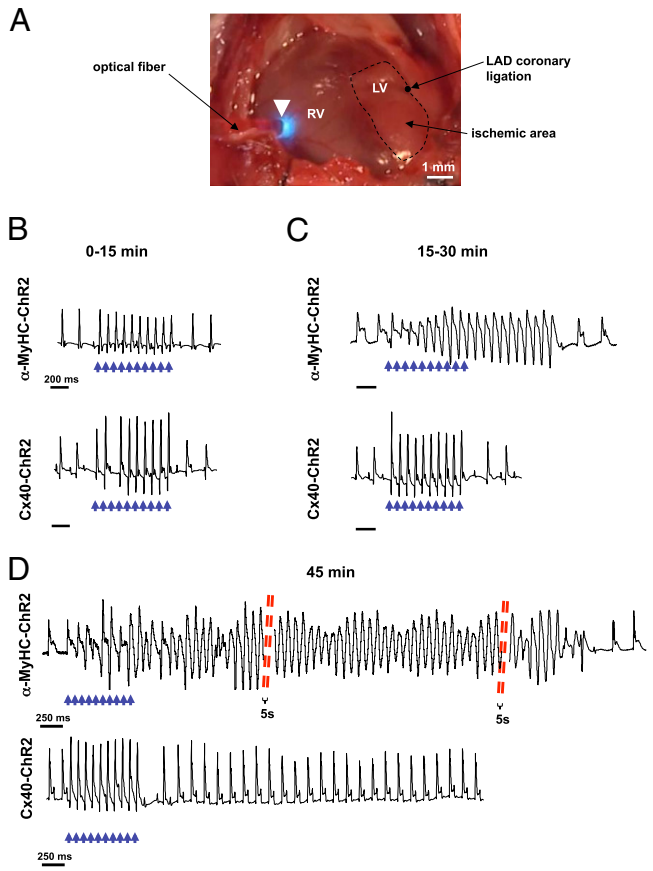

Fig. 7. Induction of sustained ventricular arrhythmias by optical stimulation in the advanced postischemic phase. (*A*) Photograph of the optogenetic experiment, picturing the heart of the anesthetized mouse, seen through the toracotomic window, during delivery of a light pulse to the RV epicardium via the optical fiber. The white arrowhead shows the heart region described in Fig. 4 *C–F*. (*B*) Representative ECG traces of RV photostimulation during the first 15 min after LAD ligation in α-MyHC-ChR2 (*Top*) and Cx40-ChR2 (*Bottom*) hearts (n = 10 and 8 mice, respectively). (*C*) Representative ECG trace recorded between 15 and 30 min after LAD ligation in α-MyHC-ChR2 (*Top*) mice. Photostimulation of the origin of the RVOT induced episodes of unsustained polymorphic VT. The *Bottom* panel shows a representative ECG trace recorded between 15 and 30 min after LAD ligation in Cx40-ChR2 mice. Blue arrows indicate the light pulses. (*D*) The *Top* panel shows a representative ECG trace of sustained arrhythmias originated by light stimulation of the RV, at the site indicated above and described in Fig. 4 *C–F*, in α-MyHC-ChR2 mice during postischemic phase 2. Sustained arrhythmias were induced in 8 out of 10 mice. The same photostimulation protocol failed to trigger sustained arrhythmias in Cx40-ChR2 mice (n = 8 mice) (*Bottom* panel). Blue arrows indicate the light pulses.

Top). Such behavior was never evoked by applying the identical stimulation protocol in the Cx40-ChR2 mice (Fig. 7 *C*, *Bottom*) (n = 6 mice for each group). Interestingly, during the transitional phase to irreversible ischemic damage (45–60 min after LAD ligation) (59–61), photostimulation of the same region of the RV triggered sustained polymorphic VT and VT/VF, lasting up to 50 s, in 8 out of 10 of the α-MyHC-ChR2 mice analyzed (Fig. 7 *D*, *Top*). On the contrary, the same protocol applied to all other myocardial areas explored, outside this region, failed to evoke sustained VT/VF. Moreover, the arrhythmia protocol applied to stimulate the Purkinje fibers of ischemic Cx40-ChR2 hearts never induced sustained arrhythmias, regardless of the stimulation frequency and location (Fig. 7 *D*, *Bottom*). In sham-operated mice (n = 4), photostimulation, either in single pulses or in bursts, never triggered sustained arrhythmias.

These results indicate that, during LV myocardial ischemia, the propensity of focal ectopic beats to trigger arrhythmias varies with the anatomical sites, as identical ectopies had remarkably different effects, ranging from single stimulated beats to the triggering of sustained arrhythmias. The highest arrhythmogenic potential was found for ectopies occurring in the region corresponding to the root of the RVOT and involving both Purkinje fibers and working cardiomyocytes. The depolarization of the sole Purkinje fibers was, in fact, not able to trigger sustained arrhythmias.

Discussion

Most ventricular arrhythmias are caused by the combined effect of factors creating a substrate in the heart tissue favoring electrical instability, with events of localized depolarization in the cardiomyocytes serving as a trigger (4, 5). Although great progress has been made in the identification of the mechanisms determining the proarrhythmogenic substrate (e.g., genetic mutations altering the single-cell electrophysiology or cell–cell communication, myocardial fibrosis) (6, 7, 60), the fundamental requirements of arrhythmia triggers are as yet poorly understood. Cardiac optogenetics was used to define such requirements by determining the minimal cell number of working versus conducting cardiomyocytes that characterize a trigger focus of ectopic heartbeats in the normal heart. The arrhythmogenic potential of such ectopies was explored during acute myocardial ischemia, a condition associated with increased arrhythmia susceptibility (9, 12, 13). In this study, the optogenetic approach discriminated with high precision the location of arrhythmia trigger sites in the heart and the different cell systems involved (working versus conducting cardiomyocytes).

Critical Determinants of Arrhythmogenic Foci. Ectopic heartbeats are common disturbances of the heart rhythm whereby the untimely depolarization of groups of cardiomyocytes, mainly due to early or delayed afterdepolarizations, disrupts the physiologic sequence of impulse formation resulting in premature contractions. The electrotonic coupling of the myocardium protects against the propagation of arrhythmogenic action potentials triggered by afterdepolarizations; only after a sufficient number of cardiomyocytes are activated simultaneously to overcome the source-sink mismatch will an ectopic beat occur (4, 5). Here we quantitatively studied the critical determinants of arrhythmogenic focal sources, including the minimal cell number, their cardiac topology, and the type of cells involved. These aspects have, thus far, only indirectly been estimated in ex vivo preparations or with simulation modeling based on cellular data (4, 5). We used optogenetics that allowed the direct activation of selective cardiac cell populations expressing the photoactivable channels (i.e., ChR2 in this study) in confined regions of the heart wall, thus mimicking focal spontaneous electrical activity. As a prerequisite to our experimentation, we determined the attenuation of the blue light across the myocardial wall, by combining light penetrance data in tissue with mathematical modeling, and were thus able to accurately control the 3D size of the ectopic foci. Our data demonstrated that the minimal number of cardiomyocytes required to form a focal ectopic site of ventricular activation is, in the mouse heart, in the order of a few thousand (from 1,300 to 1,800) cells. When premature depolarization was selectively induced in the Purkinje fiber cells, a much lower number of simultaneously depolarizing cells (in the order of 100) was needed to trigger ventricular activation. Given the highly heterogenous distribution of Purkinje fibers throughout the myocardial walls, the estimate must be taken with a broader confidence interval than in the case of working cardiomyocytes. However, this observation is in agreement with the prediction of simulation modeling (4) suggesting that, irrespective of their sensitivity to develop afterdepolarizations, conducting cardiomyocytes more easily overcome the protective

effect of myocardial current sinks, solely due to their quasi-monodimensional arrangement. Taken together, these results demonstrate that the selective optogenetic interrogation of the Purkinje fibers, combined with the topological study of their distribution, informs on the structure/function relationship of this cardiac subsystem with unprecedented detail.

Triggered Arrhythmias During Myocardial Ischemia. Acute myocardial ischemia is a major cause of SCD (9, 10). The sudden cessation of myocardial blood flow causes heterogeneities in excitability, refractoriness, and/or conduction. All of these factors contribute to creating the proarrhythmogenic myocardial substrate that, in the presence of ectopic excitation from focal sources, may trigger the lethal ventricular arrhythmias (12, 61, 62). Having established the tissue determinants for the generation of focal ectopic beats, we ascertained the characteristics of focal ectopic triggers of ventricular arrhythmias potentially causing SCD by coupling optogenetic investigation to the experimental model of acute myocardial ischemia. Central to such an experimental design, the optogenetic investigation is noninvasive and does not associate with heterogeneity in myocardial depolarization nor with tissue damage that might be caused by the production of damaging gases (Cl_2, H_2, O_2) and pH alterations during conventional electric stimulation (63, 64), especially during prolonged experiments. Focal ventricular pacing at various regions in the healthy heart could be performed even at an elevated rate and for a prolonged period (up to 30 min) and never trigger arrhythmic episodes. Local deep tissue pacing during myocardial ischemia triggered instead several arrhythmia types, progressing from short runs of extra beats to sustained VT/VF, along with ischemia time. Remarkably, the longer and more complex arrhythmias were triggered by local pacing in correspondence to the RV portion showing a complex organization in the terminal Purkinje fibers. Interestingly, the same structure has been identified in the human heart (65, 66), and it is tempting to speculate that such anatomical organization of the cardiac conduction system network might contribute to the generation of arrhythmias triggered by ectopies arising from the RVOT, as well-reported in the literature (67).

Limitations and Perspectives of the Study. The study applies cardiac optogenetics to a murine model of cardiovascular pathology (i.e., myocardial ischemia) and describes the focal arrhythmia trigger determinants. The main limitation of the study is that, although the genetic restriction of ChR2 expression to atrial and conduction system cells allowed us to selectively interrogate the Purkinje fiber function, in the alternative model used, the α-MyHC promoter drives ChR2 expression to all cardiomyocyte types and not solely to the working cardiomyocytes. We aimed to overcome such a disadvantage by combining optogenetics with the conventional pharmacologic strategy used to ablate Purkinje fibers, in a subset of experiments. Such an approach, however, could not be applied to the in vivo assessments during ischemia, due to the complex adverse effects of the treatment. The study methodology and the accuracy of the estimates of the cell number needed to generate PVCs rely centrally on the measurements of tissue light absorption. One limitation of such measures is that they have been performed using cardiac slices that, although freshly cut, are not physiologically perfused by the blood, which may have a modest but noticeable effect on tissue light penetration.

The protocols developed in the current investigation can potentially be combined to emerging methods of voltage imaging of the heart in vivo, to define in higher detail the electrophysiologic effect of local photoactivation and the mechanisms of arrhythmia dynamics. We have used here a rather simple hardware setup for the photoactivation experiments in the mouse, but our preliminary investigations indicate that technical strategies allowing complex light patterns (e.g., multiple photopacing foci or delivery of complex spatial illumination patterns) can be used to mimic relevant arrhythmogenic phenotypes, including bidirectional VTs or spiral depolarization wavefronts. In addition, a stable implant of miniaturized LED in the mouse thorax can be pursued to achieve optical stimulation of PVCs in the freely moving animal, allowing the investigation of the effects of focal ectopies in chronic disease models and the longitudinal study of drug effects.

Conclusions. In essence, our study extended the cardiac optogenetics toolkit with a murine model with ChR2 expression restricted to the conduction system and developed experimental protocols to address physiological and pathological mechanisms relevant to the understanding of cardiac arrhythmias. In perspective development, optogenetics can be used for the study of other arrhythmia-linked genetic (e.g., LQTS, CPVT) or acquired arrhythmogenic conditions and for pharmacological research aimed at the identification and testing of antiarrhythmic compounds.

Methods

Mouse Models. For ex vivo study, we used transgenic adult (3 mo old) male mice expressing the hChR2(H134R)-*td*Tomato fusion gene under the control of the α-MyHC promoter; mice were backcrossed into the C57B6J background. For in vivo study, transgenic adult male mice, with a genetic background C57B6J, expressing cre-recombinase under the control of either the α-MyHC or Cx40 promoter were bred with B6.Cg-Gt(ROSA)26Sor$^{tm27.1(CAG-COP4*H134R/tdTomato)Hze}$/J-expressing mice (Jackson Lab). The resulting offspring had the STOP cassette deleted in the heart, resulting in cardiomyocyte (α-MyHC-ChR2) or Purkinje fiber (Cx40-ChR2) expression of the hChR2(H134R)-*td*Tomato fusion protein. Both α-MyHC-cre$^{+/-}$ and Cx40-cre$^{+/-}$ lines were used to maintain the colonies. Hearts from Cx40-GFP transgenic mice were also analyzed (68). All experimental procedures described in this article have been approved by the institutional ethical committee, Comitato Etico di Ateneo per la Sperimentazione Animale, University of Padova (authorization C54) and communicated to the relevant Italian authority (Ministero della Salute, Ufficio VI), in compliance with Italian Animal Welfare Law (Laws n 116/1992, D.Lgs 26/2014, and subsequent modifications).

Optical Mapping. The electrical activity of hearts of transgenic ChR2 mice was visualized in Langendorff isolated perfused hearts, via epicardial voltage mapping. To eliminate cross-talk between stimulating light and fluorescence emission, the dye RH1691 (40 μM), which has a deep red emission spectrum, was used. The recording system consisted of the commercially available microscope MVX10 (Olympus) and the MiCam camera system, which allows recording with a frame rate of up to 1 kHz at a spatial resolution of 100 × 100 pixels. As the light source for the photostimulation, a high-power LED with an emitting peak wavelength of 470 nm was coupled to multimode optical fibers (Thorlabs GmbH) with decreasing diameters (1,000 μm, 800 μm, 400 μm, and 200 μm). The LED was triggered via a high-power, one-channel LED driver with pulse modulation (Thorlabs GmbH). Signals were analyzed applying custom-made software (MatLab, Mathworks).

In Vivo Epicardial Photostimulation. Adult ChR2-expressing transgenic male mice and littermate controls were anesthetized by isoflurane administration (1.5–3% vol/vol), secured to the table in supine position, and intubated with a 24G needle for ventilation (tidal volume, 0.4 mL; 120 strokes per minute) from an artificial ventilator (SAR-830). Body temperature was monitored constantly during the experiment. The skin was dissected by a lateral subascellary 1.5-cm cut, s.c. muscles were removed, and a 0.5-cm incision was performed at the level of the fourth intercostal space. Self-retaining microretractors were then used to separate the third and fourth ribs enough to get adequate exposure of the operating region. The heart was exposed and different epicardial regions from the atria and the LVs and RVs were stimulated by differently sized (from 100 to 1,500 diameter, in μm) fiber optics (Thorlabs), coupled to a 470-nm LED (Thorlabs), controlled by an ECG-coupled recording system (Powerlab 8/30, Bioamp and LabChart 7.1 software; AD Instruments). Trains of 5-ms light pulses were delivered with a cycle length of 100 ms, with the exception of the burst stimulation used for the study of arrhythmia triggering.

ECG Recording and Analysis. A standard lead I ECG was recorded (Powerlab 8/30, Bioamp; AD Instruments) during the experiment. ECG parameters (QRS, PR interval and heart rate) were calculated by using LabChart 7.1 software (AD Instruments).

Measurement of the Ventricular ERP. The ventricular ERP (VERP) of both the working cardiomyocytes and Purkinje fibers was evaluated in α-MyHC-ChR2 and Cx40-ChR2, respectively, by using the extrastimulus technique (69, 70). The epicardial surface of the RV was photostimulated by a train of 10 light pulses (5 ms), at a frequency of 10 Hz (cycle length, 100 ms) (S1), followed by a premature optical stimulus (S2) at a progressively shorter coupling interval until the S2 failed to trigger an ectopy at the VERP (Fig. 5*B*).

Burst Photoactivation Protocol. Brief trains of 5-ms light pulses were delivered to a fixed epicardial region with repetition rates ranging from 10 Hz to 25 Hz (cycle length, 100 ms to 40 ms). For each experiment, stimulation was delivered to five reference regions at the heart base and mid portion, which specifically were as follows: 1, LV anterior; 2, LV septal; 3, lateral; 4, RV free wall; 5, septal. The apex was considered separately.

Pharmacological Purkinje Fiber Ablation. We carefully injected 10 μL of Lugol's solution [5% (wt/v) iodine and 10% (wt/v) potassium iodide, in distilled water] supplemented with an equal volume of Heparin (all from SIGMA) into either the RV or the LV cavity by using a Hamilton syringe supporting a 34G needle. To increase permanence of Lugol's solution in the ventricles, the pulmonary artery or the aorta was transiently clamped (about 10 s).

Optical Projection Tomography. Hearts from Cx40-GFP transgenic mice were analyzed as previously described in ref. 71.

LAD Coronary Artery Ligation. The main trunk of the LAD coronary artery was ligated under microscope guidance, by using a 7/0 polypropylene suture (72). Epicardial photostimulation was performed at different time points (from 5 to 90 min) after coronary occlusion, during constant ECG recording.

Measurement of Blue Light Attenuation in the Myocardium. Hearts from both control and ChR2-expressing mice were harvested, and the LV and RV walls dissected. Intact ventricles, as well as longitudinally cut ventricular slices of different thickness, were placed in contact with the light sensor of a power meter (Thorlabs, PM100D). The same fiber optics used in the in vivo experiments were used to determine tissue light attenuation, by illuminating the slices while measuring the emerging light intensity with the power meter. Emerging light intensity was measured for each fiber diameter (from 100 to 1,500 μm), at varying light intensities (from 0.36 to 27 mW/mm^2), and all these measures were performed in slices of different thickness (from 25 to 800 μm). Myocardial light attenuation was modeled by adapting previous studies made in the brain (57). Briefly, values of light intensity experimentally determined using the tissue phantoms described above were fitted to a monoexponential decay curve to extrapolate light intensity as a function of the depth from the epicardial surface. The light intensity threshold for ChR2 activation was obtained from refs. 35, 37. To determine the lateral discrimination of the illuminating beam in the myocardium, slices were imaged through a modified inverted microscope (Nikon Eclipse 200) equipped with a 2048 × 1024 pixel CCD detector (Hamamatsu) to acquire the image of the fiber optic carrying 470 nm light, as emerging through myocardial tissue samples of incremental thickness. In each image, the shape, brightness, pixel intensity distribution, and intensity linear profile were calculated using image analysis software (ImageJ, Wayne Rasband, NIH).

Tissue Samples and Immunofluorescence Analysis. The hearts were harvested from transgenic as well as control mice, fixed in 2% (wt/vol) paraformaldehyde (Sigma) for 1 h at room temperature, equilibrated in sucrose gradient at 4 °C, embedded in OCT, and frozen in liquid nitrogen. We obtained 10-μm myocardial sections with a cryostat (Leica CM1850, Leica Microsystems GmbH) and processed them for histological and immunofluorescence analyses. Immunofluorescence analysis was performed as described in ref. 73. The following primary antibodies were used in this study: rabbit anti-cx40 (1:200, Invitrogen) and mouse anti–α-MyHC (1:200, clone BAG5) (74). FITC-conjugated secondary antibodies, all from Jackson Laboratory, were used to detect primary antibodies. Sections were analyzed with a Leica TCS SP5 confocal microscope.

Statistical Analysis. All data are expressed as the mean ± SEM. Comparison between the experimental groups was made by using the nonpaired Student's *t* and ANOVA tests followed by Bonferroni correction, with $P < 0.05$ being considered statistically significant.

ACKNOWLEDGMENTS. We are grateful to Godfrey Smith, Robert Kelly, Tullio Pozzan, Nicola Elvassore, Leonardo Sacconi, Davide Gobbo, and Niccolò Roda for critical discussion and Anna Pia Plazzo and Emilio Bigon for technical assistance. This work was supported by the following grants: the European Community Seventh Framework Program FP7/2007-2013 under Grant Agreement HEALTH-F2-2009-241526, EUTrigTreat (to M.M., S.L., and S.E.L.), Deutsche ForschungsGemeinschaft SFB 1002 TP B05 (to S.E.L.), and Telethon-Italy GGP11224 (to M.M.).

1. Sedmera D, Gourdie RG (2014) Why do we have Purkinje fibers deep in our heart? *Physiol Res* 63(Suppl 1):S9–S18.
2. Hoyt RH, Cohen ML, Saffitz JE (1989) Distribution and three-dimensional structure of intercellular junctions in canine myocardium. *Circ Res* 64(3):563–574.
3. Rohr S, Kucera JP, Fast VG, Kléber AG (1997) Paradoxical improvement of impulse conduction in cardiac tissue by partial cellular uncoupling. *Science* 275(5301):841–844.
4. Xie Y, Sato D, Garfinkel A, Qu Z, Weiss JN (2010) So little source, so much sink: Requirements for afterdepolarizations to propagate in tissue. *Biophys J* 99(5):1408–1415.
5. Myles RC, Wang L, Kang C, Bers DM, Ripplinger CM (2012) Local β-adrenergic stimulation overcomes source-sink mismatch to generate focal arrhythmia. *Circ Res* 110(11):1454–1464.
6. Wilders R, et al. (2000) Effects of anisotropy on the development of cardiac arrhythmias associated with focal activity. *Pflugers Arch* 441(2-3):301–312.
7. Peters NS, Wit AL (1998) Myocardial architecture and ventricular arrhythmogenesis. *Circulation* 97(17):1746–1754.
8. Goldberger JJ, et al.; American Heart Association; American College of Cardiology Foundation; Heart Rhythm Society (2008) American Heart Association/American College of Cardiology Foundation/Heart Rhythm Society scientific statement on noninvasive risk stratification techniques for identifying patients at risk for sudden cardiac death: A scientific statement from the American Heart Association Council on Clinical Cardiology Committee on Electrocardiography and Arrhythmias and Council on Epidemiology and Prevention. *Circulation* 118(14):1497–1518.
9. Campbell RW, Murray A, Julian DG (1981) Ventricular arrhythmias in first 12 hours of acute myocardial infarction. Natural history study. *Br Heart J* 46(4):351–357.
10. Zheng ZJ, Croft JB, Giles WH, Mensah GA (2001) Sudden cardiac death in the United States, 1989 to 1998. *Circulation* 104(18):2158–2163.
11. Cerrone M, et al. (2007) Arrhythmogenic mechanisms in a mouse model of catecholaminergic polymorphic ventricular tachycardia. *Circ Res* 101(10):1039–1048.
12. Bogun F, et al. (2006) Role of Purkinje fibers in post-infarction ventricular tachycardia. *J Am Coll Cardiol* 48(12):2500–2507.
13. Hayashi M, et al. (2006) Novel mechanism of postinfarction ventricular tachycardia originating in surviving left posterior Purkinje fibers. *Heart Rhythm* 3(8):908–918.
14. Herron TJ, Milstein ML, Anumonwo J, Priori SG, Jalife J (2010) Purkinje cell calcium dysregulation is the cellular mechanism that underlies catecholaminergic polymorphic ventricular tachycardia. *Heart Rhythm* 7(8):1122–1128.
15. Boyden PA, Hirose M, Dun W (2010) Cardiac Purkinje cells. *Heart Rhythm* 7(1): 127–135.
16. Kang G, et al. (2010) Purkinje cells from RyR2 mutant mice are highly arrhythmogenic but responsive to targeted therapy. *Circ Res* 107(4):512–519.
17. Scheinman MM (2009) Role of the His-Purkinje system in the genesis of cardiac arrhythmia. *Heart Rhythm* 6(7):1050–1058.
18. Li P, Rudy Y (2011) A model of canine purkinje cell electrophysiology and Ca(2+) cycling: Rate dependence, triggered activity, and comparison to ventricular myocytes. *Circ Res* 109(1):71–79.
19. Syed FF, Hai JJ, Lachman N, DeSimone CV, Asirvatham SJ (2014) The infrahisian conduction system and endocavitary cardiac structures: Relevance for the invasive electrophysiologist. *J Interv Card Electrophysiol* 39(1):45–56.
20. Davidenko JM, Antzelevitch C (1986) Electrophysiological mechanisms underlying rate-dependent changes of refractoriness in normal and segmentally depressed canine Purkinje fibers. The characteristics of post-repolarization refractoriness. *Circ Res* 58(2):257–268.
21. Wellens HJ (2008) Forty years of invasive clinical electrophysiology: 1967-2007. *Circ Arrhythm Electrophysiol* 1(1):49–53.
22. Saba S, Wang PJ, Estes NA, 3rd (2000) Invasive cardiac electrophysiology in the mouse: Techniques and applications. *Trends Cardiovasc Med* 10(3):122–132.
23. Ward DE, Camm AJ (1980) Methodologic problems in the use of atrial pacing studies for the assessment of A-V conduction. *Clin Cardiol* 3(3):155–162.
24. Peters RW, Scheinman MM, Raskin S, Desai J (1979) Determination of His-Purkinje refractoriness in man with His bundle pacing. *Circulation* 60(4):956–959.
25. Pang BJ, Kumar S, Tacey MA, Mond HG (2014) Capturing the His-Purkinje system is not possible from conventional right ventricular apical and nonapical pacing sites. *Pacing Clin Electrophysiol* 37(6):724–730.
26. Fenno L, Yizhar O, Deisseroth K (2011) The development and application of optogenetics. *Annu Rev Neurosci* 34:389–412.
27. Boyden ES, Zhang F, Bamberg E, Nagel G, Deisseroth K (2005) Millisecond-timescale, genetically targeted optical control of neural activity. *Nat Neurosci* 8(9):1263–1268.
28. Plazzo AP, et al. (2012) Bioinformatic and mutational analysis of channelrhodopsin-2 protein cation-conducting pathway. *J Biol Chem* 287(7):4818–4825.
29. Zhang F, Aravanis AM, Adamantidis A, de Lecea L, Deisseroth K (2007) Circuit-breakers: Optical technologies for probing neural signals and systems. *Nat Rev Neurosci* 8(8):577–581.
30. Zhang F, et al. (2007) Multimodal fast optical interrogation of neural circuitry. *Nature* 446(7136):633–639.

31. Chow BY, Han X, Boyden ES (2012) Genetically encoded molecular tools for light-driven silencing of targeted neurons. *Prog Brain Res* 196:49–61.
32. Abilez OJ (2012) Cardiac optogenetics. *Conf Proc IEEE Eng Med Biol Soc* 2012: 1386–1389.
33. Entcheva E (2013) Cardiac optogenetics. *Am J Physiol Heart Circ Physiol* 304(9): H1179–H1191.
34. Arrenberg AB, Stainier DY, Baier H, Huisken J (2010) Optogenetic control of cardiac function. *Science* 330(6006):971–974.
35. Bruegmann T, et al. (2010) Optogenetic control of heart muscle in vitro and in vivo. *Nat Methods* 7(11):897–900.
36. Boyle PM, Entcheva E, Trayanova NA (2014) See the light: Can optogenetics restore healthy heartbeats? And, if it can, is it really worth the effort? *Expert Rev Cardiovasc Ther* 12(1):17–20.
37. Boyle PM, Williams JC, Ambrosi CM, Entcheva E, Trayanova NA (2013) A comprehensive multiscale framework for simulating optogenetics in the heart. *Nat Commun* 4:2370.
38. Sasse P (2011) Optical pacing of the heart: The long way to enlightenment. *Circ Arrhythm Electrophysiol* 4(5):598–600.
39. Nussinovitch U, Shinnawi R, Gepstein L (2014) Modulation of cardiac tissue electrophysiological properties with light-sensitive proteins. *Cardiovasc Res* 102(1):176–187.
40. Jia Z, et al. (2011) Stimulating cardiac muscle by light: Cardiac optogenetics by cell delivery. *Circ Arrhythm Electrophysiol* 4(5):753–760.
41. Beiert T, Bruegmann T, Sasse P (2014) Optogenetic activation of Gq signalling modulates pacemaker activity of cardiomyocytes. *Cardiovasc Res* 102(3):507–516.
42. Beyer S, Kelly RG, Miquerol L (2011) Inducible Cx40-Cre expression in the cardiac conduction system and arterial endothelial cells. *Genesis* 49(2):83–91.
43. Cha YM, et al. (1995) Effects of chemical subendocardial ablation on activation rate gradient during ventricular fibrillation. *Am J Physiol* 269(6 Pt 2):H1998–H2009.
44. Chen PS, Wolf PL, Cha YM, Peters BB, Topham SL (1993) Effects of subendocardial ablation on anodal supernormal excitation and ventricular vulnerability in open-chest dogs. *Circulation* 87(1):216–229.
45. Damiano RJ, Jr, et al. (1986) The effect of chemical ablation of the endocardium on ventricular fibrillation threshold. *Circulation* 74(3):645–652.
46. Uhley HN, Rivkin LM (1959) Visualization of the left branch of the human atrioventricular bundle. *Circulation* 20:419–421.
47. Taufic M, Bashour FA, Lewis FJ (1955) Production of heart block in dogs, under direct vision. *Surg Forum* 5:96–101.
48. Robinson RB, Boyden PA, Hoffman BF, Hewett KW (1987) Electrical restitution process in dispersed canine cardiac Purkinje and ventricular cells. *Am J Physiol* 253(5 Pt 2): H1018–H1025.
49. Bailey JC, Lathrop DA, Pippenger DL (1977) Differences between proximal left and right bundle branch block action potential durations and refractoriness in the dog heart. *Circ Res* 40(5):464–468.
50. Carmeliet E (1980) Electrophysiological effects of encainide on isolated cardiac muscle and Purkinje fibers and on the Langendorff-perfused guinea-pig heart. *Eur J Pharmacol* 61(3):247–262.
51. Persson F, Andersson B, Duker G, Jacobson I, Carlsson L (2007) Functional effects of the late sodium current inhibition by AZD7009 and lidocaine in rabbit isolated atrial and ventricular tissue and Purkinje fibre. *Eur J Pharmacol* 558(1-3):133–143.
52. Denker S, Lehmann M, Mahmud R, Gilbert C, Akhtar M (1984) Effects of alternating cycle lengths on refractoriness of the His-Purkinje system. *J Clin Invest* 74(2):559–570.
53. Denker S, Shenasa M, Gilbert CJ, Akhtar M (1983) Effects of abrupt changes in cycle length on refractoriness of the His-Purkinje system in man. *Circulation* 67(1):60–68.
54. Martin CA, Grace AA, Huang CL (2011) Refractory dispersion promotes conduction disturbance and arrhythmias in a Scn5a (+/-) mouse model. *Pflugers Arch* 462(4): 495–504.
55. Deng W, Goldys EM, Farnham MM, Pilowsky PM (2014) Optogenetics, the intersection between physics and neuroscience: Light stimulation of neurons in physiological conditions. *Am J Physiol Regul Integr Comp Physiol* 307(11):R1292–R1302.
56. Hall G, Jacques SL, Eliceiri KW, Campagnola PJ (2012) Goniometric measurements of thick tissue using Monte Carlo simulations to obtain the single scattering anisotropy coefficient. *Biomed Opt Express* 3(11):2707–2719.
57. Aravanis AM, et al. (2007) An optical neural interface: In vivo control of rodent motor cortex with integrated fiberoptic and optogenetic technology. *J Neural Eng* 4(3): S143–S156.
58. Roy A, Ramasubramaniam R, Gaonkar HA (2012) Empirical relationship between Kubelka-Munk and radiative transfer coefficients for extracting optical parameters of tissues in diffusive and nondiffusive regimes. *J Biomed Opt* 17(11):115006.
59. Mesradi M, et al. (2013) Experimental and analytical comparative study of optical coefficient of fresh and frozen rat tissues. *J Biomed Opt* 18(11):117010.
60. Peters NS (1996) New insights into myocardial arrhythmogenesis: Distribution of gap-junctional coupling in normal, ischaemic and hypertrophied human hearts. *Clin Sci (Lond)* 90(6):447–452.
61. Clements-Jewery H, Hearse DJ, Curtis MJ (2005) Phase 2 ventricular arrhythmias in acute myocardial infarction: A neglected target for therapeutic antiarrhythmic drug development and for safety pharmacology evaluation. *Br J Pharmacol* 145(5): 551–564.
62. Takahashi Y, Takahashi A, Isobe M (2008) Ventricular fibrillation initiated by premature beats from the ventricular myocardium not associated with the Purkinje system after myocardial infarction. *Heart Rhythm* 5(10):1458–1460.
63. Merrill DR, Bikson M, Jefferys JG (2005) Electrical stimulation of excitable tissue: Design of efficacious and safe protocols. *J Neurosci Methods* 141(2):171–198.
64. Wikswo JP, Jr, Lin SF, Abbas RA (1995) Virtual electrodes in cardiac tissue: A common mechanism for anodal and cathodal stimulation. *Biophys J* 69(6):2195–2210.
65. Atkinson A, et al. (2011) Anatomical and molecular mapping of the left and right ventricular His-Purkinje conduction networks. *J Mol Cell Cardiol* 51(5):689–701.
66. Tusscher KH, Panfilov AV (2008) Modelling of the ventricular conduction system. *Prog Biophys Mol Biol* 96(1-3):152–170.
67. Dobrzynski H, et al. (2013) Structure, function and clinical relevance of the cardiac conduction system, including the atrioventricular ring and outflow tract tissues. *Pharmacol Ther* 139(2):260–288.
68. Miquerol L, et al. (2004) Architectural and functional asymmetry of the His-Purkinje system of the murine heart. *Cardiovasc Res* 63(1):77–86.
69. Han J, Moe GK (1964) Nonuniform recovery of excitability in ventricular muscle. *Circ Res* 14:44–60.
70. Burton FL, Cobbe SM (2001) Dispersion of ventricular repolarization and refractory period. *Cardiovasc Res* 50(1):10–23.
71. Miquerol L, et al. (2010) Biphasic development of the mammalian ventricular conduction system. *Circ Res* 107(1):153–161.
72. Ahn D, et al. (2004) Induction of myocardial infarcts of a predictable size and location by branch pattern probability-assisted coronary ligation in C57BL/6 mice. *Am J Physiol Heart Circ Physiol* 286(3):H1201–H1207.
73. Zaglia T, et al. (2013) Cardiac sympathetic neurons provide trophic signal to the heart via β2-adrenoceptor-dependent regulation of proteolysis. *Cardiovasc Res* 97(2): 240–250.
74. Rudnicki MA, Jackowski G, Saggin L, McBurney MW (1990) Actin and myosin expression during development of cardiac muscle from cultured embryonal carcinoma cells. *Dev Biol* 138(2):348–358.